JOURNAL OF SOLID STATE CHEMISTRY 108, 170–176 (1994)

Structure of $MoO_3 \cdot 1/2H_2O$ by Conventional X-Ray Powder Diffraction

P. Bénard,* L. Seguin,† D. Louër,* and M. Figlarz†

*Laboratoire de Cristallochimie, URA CNRS 1495, Université de Rennes I, Avenue du Général Leclerc, 35042 Rennes Cedex, France; and †Laboratoire de Réactivité et de Chimie des Solides, URA CNRS 1211, Université de Picardie, 33, rue Saint-Leu, 80039 Amiens Cedex, France

Received February 17, 1993; in revised form April 30, 1993; accepted May 13, 1993

The crystal structure of the compound $MoO_3 \cdot 1/2H_2O$ was solved ab initio from conventional X-ray powder diffraction data and refined by the Rietveld method. This hydrate crystallizes in the monoclinic space group $P2_1/m$ with unit cell dimensions $a = 9.6715(2)$ Å, $b = 3.70518(7)$ Å, $c = 7.0975(1)$ Å, $\beta = 102.403(1)°$, and $V = 248.40(1)$ Å^3, for $Z = 4$; 137 integrated intensities obtained by an iterative method were used to generate a Patterson map from which the initial positional parameters of two independent molybdenum atoms were derived. The remaining nonhydrogen atoms were located by Fourier methods. Refinement of the complete diffraction profile parameters (44 parameters, 575 reflections) converged to final agreement factors $R_p = 0.088$, $R_{wp} = 0.113$, and $R_F = 0.021$. The structure consists of isolated layers parallel to (001), formed by double linear rows running along [010] and linked together through corner-sharing $[MoO_6]$ and $[MoO_5(H_2O)]$ octahedra. A double chain is built up from strongly distorted $[MoO_6]$ octahedra sharing two common edges with each other, and the next one is in a similar layer, but with $[MoO_5(H_2O)]$ octahedra. The successive layers are held together by hydrogen bonding to form a two-dimensional network.

INTRODUCTION

Studies on the structural chemistry of molybdenum trioxide and related hydrated phases have been reviewed by Hulliger (1). The structure of a few hydrates has been established; among them are a monoclinic dihydrate $MoO_3 \cdot 2H_2O$ (2, 3), a white triclinic monohydrate α-$MoO_3 \cdot H_2O$ (4, 5), and a yellow monoclinic modification β-$MoO_3 \cdot H_2O$ (6). Two other hydrated phases have also been reported, the orthorhombic $MoO_3 \cdot 1/3H_2O$ (7) and the monoclinic hemihydrate $MoO_3 \cdot 1/2H_2O$ (8). The structure of $MoO_3 \cdot 1/3H_2O$ has been established from X-ray powder data, by analogy with $WO_3 \cdot 1/3H_2O$, and confirmed by IR spectroscopy (7); to our knowledge the crystal structure of $MoO_3 \cdot 1/2H_2O$ is still unknown. An X-ray diffraction study of the hemihydrate has been reported by Fellows *et al.* (8), in which the parameters of the monoclinic cell were determined. Although a single crystal of this phase could be isolated by these authors, it seems that no result on the crystal structure of this material was reported. This can probably be explained by the fibrous habit of the crystals. On the other hand, the feasibility of carrying out structural analyses of powder materials, with unknown structure, has now been demonstrated in a number of studies, from data collected with X-ray synchrotron source (9, 10) and conventional sealed-tube X-ray source (11–13). These new developments of powder crystallography have been applied to investigate the structure of the hemihydrate $MoO_3 \cdot 1/2H_2O$. The results of the ab initio structure determination of this phase from data collected by means of a conventional X-ray source are presented in this paper.

EXPERIMENTAL

Synthesis. To prepare the $MoO_3 \cdot 1/2H_2O$ sample, a modified version of the method reported by Fellows *et al.* (8) has been used. It has been prepared by dissolving molybdenum powder (Prolabo purity 99,9%) in 3 *M* nitric acid in order to obtain a molybdenum concentration of 0.23 *M*. Since a brown precipitate of MoO_2 appears, the solution is recovered by filtration. Then concentrated nitric acid is added to this colorless solution in order to obtain a solution of 0.175 *M* molybdenum in 6 *M* nitric acid. The solution is stirred by magnetic agitation at 60°C. After 3 days a white precipitate appears, the quantity of which no longer increases after 1 week. The white precipitate is washed with water and alcohol, and dried at room temperature. By this method, the $MoO_3 \cdot 1/2H_2O$ obtained is pure and with a crystallinity good enough to solve the structure by X-ray powder diffraction.

A thermogravimetric analysis has been performed to verify the water content. The mass loss measured from this curve confirms that the stoichiometry is $MoO_3 \cdot 1/2H_2O$.

X-ray diffraction data collection. A D500 Siemens powder diffractometer, using Bragg–Brentano geometry,

0022-4596/94 $6.00

was used for data collection. Pure monochromatic Cu$K\alpha_1$ radiation (λ = 1.540598 Å) was selected by means of an incident beam curved-crystal germanium monochromator with asymmetric focusing (short focal distance 124 mm, long focal distance 216 mm). The divergence slits located in the incident beam were adjusted to ensure a complete illumination of the specimen surface at about 12°(2θ). The alignment of the diffractometer was checked by means of standard reference materials. The zero error was measured as less than 0.01°(2θ). The instrumental resolution function for the diffractometer, obtained from an annealed barium fluoride sample, shows a shallow minimum in the FWHM [0.065°(2θ) at about 40°(2θ) (14)]. Throughout the experiment the ambient temperature was maintained at 296 ± 1 K. Preliminary data collections from different preparations of the sample have revealed significant preferred-orientation effects. A study of the sample by scanning electron microscopy confirmed these later observations made by X-ray diffraction and shows that the particles have a fibrous morphology with a size about 20 × 2 μm. As a consequence, in order to increase the random orientation of crystallites, the molybdenum oxide hemihydrate powder was ground and shifted. Moreover, a side-loading method of the sample holder was used. The powder diffraction pattern was scanned in steps of 0.02°(2θ), and a fixed-time counting (28 sec) was employed. At the end of the data collection the stability of the intensity of the incident beam was checked by recording the first lines of the pattern. A careful evaluation of peak positions and integrated intensities of Bragg components was carried out by means of the fitting program available in the PC software package DIFFRAC-AT supplied by Siemens/Socabim.

Structure determination and Rietveld refinement. All the calculations were performed on a MicroVAX 3100 computer. The indexing of the powder pattern is one of the determinant stages in the structural analysis, which needs high accuracy in diffraction line positions. In the present case, an absolute error less than 0.03°(2θ) was estimated for the peak position measurements. The successive dichotomy method (15), which is based on an exhaustive strategy in parameter-space, was applied to the first 20 lines observed in the powder diffraction pattern. Only one solution with a monoclinic symmetry was suggested by the program DICVOL91 (16). The high values of figures of merit (17, 18) M_{20} = 71 and F_{20} = 91(0.0065, 34) are an indication of the reliability of both the unit cell and indexing. The solution is in agreement with the result reported by Fellows *et al.* (8). The proposed unit cell indexes all the observed lines of the diffraction pattern (Table 1). Calculated data in Table 1 correspond to the unit cell parameters a = 9.675(1) Å, b = 3.7069(6) Å, c = 7.1004(8) Å, and β = 102.38(1)°, after a

TABLE 1
X-Ray Powder Diffraction Data for $MoO_3 \cdot 1/2H_2O$

$h\ k\ l$	$2\theta_{obs}$ (°)	$2\theta_{calc}$ (°)	d_{obs} (Å)	I_{obs}
0 0 1	12.737	12.754	6.94	59
$\bar{1}$ 0 1	14.092	14.116	6.28	1
1 0 1	17.370	17.394	5.10	8
2 0 0	18.742	18.765	4.73	65
$\bar{2}$ 0 1	20.335	20.331	4.364	<1
2 0 1	24.957	24.955	3.565	34
$\bar{1}$ 0 2	25.380	25.372	3.506	<1
0 0 2	25.660	25.670	3.469	21
$\bar{1}$ 1 0	25.784	25.796	3.452	6
0 1 1	27.269	27.257	3.268	<1
$\bar{1}$ 1 1	27.928	27.940	3.192	100
3 0 0	28.309	28.309	3.150	14
$\bar{2}$ 0 2 $\bar{3}$ 0 1	28.438	28.453 28.476	3.136	33
1 0 2	29.244	29.251	3.051	6
1 1 1	29.775	29.783	2.998	30
$\bar{2}$ 1 0	30.621	30.629	2.917	7
3 0 1	33.640	33.651	2.662	<1
$\bar{3}$ 0 2	34.083	34.076	2.628	<1
2 1 1	34.876	34.887	2.570	8
$\bar{1}$ 1 2 2 0 2	35.184	35.196 35.205	2.549	8
0 1 2	35.402	35.418	2.533	1
3 1 0 $\bar{4}$ 0 1	37.433	37.436 37.462	2.4005	11
$\bar{2}$ 1 2 $\bar{3}$ 1 1	37.527	37.548 37.566	2.3947	2
$\bar{1}$ 0 3 4 0 0	37.989	38.006 38.059	2.3667	<1
1 1 2	38.155	38.175	2.3568	3
0 0 3	38.917	38.928	2.3123	6
$\bar{2}$ 0 3	39.510	39.523	2.2790	18
$\bar{4}$ 0 2	41.320	41.340	2.1833	3
3 1 1	41.764	41.749	2.1611	<1
$\bar{3}$ 1 2	42.116	42.104	2.1438	<1
1 0 3	42.176	42.153	2.1409	<1
3 0 2	42.696	42.683	2.1160	6
4 0 1 2 1 2	42.978	42.975 43.052	2.1028	15
$\bar{3}$ 0 3	43.163	43.263	2.0942	<1
$\bar{4}$ 1 1	44.970	44.976	2.0142	3
$\bar{1}$ 1 3	45.444	45.446	1.9942	3
$\bar{4}$ 1 0	45.500	45.492	1.9919	1
0 1 3	46.251	46.245	1.9613	3
$\bar{2}$ 1 3	46.779	46.764	1.9404	2
$\bar{5}$ 0 1	47.019	47.006	1.9311	1
2 0 3	47.301	47.297	1.9202	2
5 0 0	48.098	48.104	1.8902	6
$\bar{4}$ 1 2	48.356	48.361	1.8807	3
$\bar{4}$ 0 3	48.832	48.815	1.8635	1
1 1 3 0 2 0	49.107	49.081 49.115	1.8537	16
3 1 2	49.562	49.552	1.8378	5
4 1 1	49.824	49.813	1.8287	7
$\bar{3}$ 1 3 1 2 0	50.067	50.070 50.114	1.8204	8
0 2 1	50.956	50.959	1.7907	3
4 0 2	51.204	51.203	1.7826	1
$\bar{1}$ 2 1	51.384	51.366	1.7768	<1
$\bar{1}$ 0 4	51.492	51.465	1.7733	<1

least-squares refinement from observed data by means the computer program NBS*AIDS83 (19). The presence of a dominant zone should be noted; indeed, the first eight consecutive lines are *h*0*l* reflections; this example demonstrates again that the successive dichotomy method is insensitive to one common zero index for all the first lines of the pattern (20). So, it is surprising to see that Fellows *et al.* (8) reported unsuccessful attempt in determining the *b* value of the unit cell of $MoO_3 \cdot 1/2H_2O$ by using the program DICVOL. This can best be explained by the lower quality of their data (see Table 1 in Ref. (8)), as shown by the corresponding figures of merit $M_{20} = 15$ and $F_{30} = 19(0.0242, 66)$ calculated by means of the program NBS*AIDS83 (19). For comparison, the dataset given in the Table 1 corresponds to figures of merit $M_{20} = 47$ and $F_{30} = 63(0.0125, 38)$. From the list of unambiguous peaks detected in the powder diffraction pattern, it was seen that all lines could be indexed using the restriction $0k0$, $k = 2n$, which is consistent with the space group $P2_1/m$. This was confirmed, as shown later, by the result of the ab initio structure determination and the Rietveld refinement of the structure.

Integrated intensities in the angular range 10–68°(2θ) were extracted by means of an iterative procedure (21), which is implemented in the program FULLPROF (22) based on the Rietveld version DBW3.2S (8804) (23), which is a successor of the program described by Wiles and Young (24); 137 F_{obs} values were obtained and used as input data in the Enraf–Nonius's structure crystallographic computing package (*MolEN*) (25) to generate a three-dimensional Patterson function, from which the approximate positions of two independent molybdenum atoms were derived. The corresponding coordinates were input in the Rietveld profile refinement method, leading to a crystal-structure model indicator $R_F = 26\%$. The strongest peaks from two successive difference-Fourier maps could be attributed to the oxygen atoms, taking into account their expected distances between them and to the heavy atoms, and also the bond angles. Finally, the positions of seven oxygen atoms were found in the asymmetric unit. At this stage, the least-squares structure refinement was continued with the Rietveld refinement. The modified-Lorentzian function was used in the initial stages of the study to describe the diffraction lines profiles and was later replaced by a pseudo-Voigt function, with a possible angular variation of the mixing parameter η. For the description of the angular dependence of the peak-full width at half-maximum, the usual quadratic form in tan θ was used with initial values of the *U*, *V*, and *W* constants calculated from components obtained by pattern decomposition. Due to the Lorentzian trend of the line shapes, integrated intensities were distributed over 11 FWHM on either side of a diffraction line. Unit cell and profile parameters were allowed to vary when the angular range increases. The final profile analysis refinement was carried out in the range 16–140°(2θ) and involved the following parameters: 18 atomic coordinates, 7 isotropic temperature factors, 1 scale factor, 1 zero-point parameter, 4 cell parameters, 3 halfwidth and 1 asymmetric parameters, 6 coefficients used to define the function dependence of the background, and 2 parameters for the description of the angular variation of the mixing factor η. The last variable to be refined was the preferred-orientation factor; it was found to be close to zero (*G*1 = 0.007), which indicates the efficiency of the sample preparation. The details of the Rietveld refinement are given in Table 2. Figure 1 shows the best fit obtained between calculated and observed patterns. This fit corresponds to satisfactory crystal-structure model indicators ($R_F = 2.1\%$, $R_B = 3.5\%$) and profile factors ($R_p = 8.8\%$, $R_{wp} = 11.3\%$). Final atomic parameters are given in Table 3 and selected bond distances and angles in Table 4. It can be noted that the isotropic temperature factors are slightly negative or zero for oxygens O(3), O(4), O(5), and

TABLE 2
Details of Rietveld Full-Profile Refinement for $MoO_3 \cdot 1/2H_2O$

a (Å)	9.6715(2)
b (Å)	3.70518(7)
c (Å)	7.0975(1)
β (°)	102.403(1)
Space group	$P2_1/m$
Z	4
Wavelength (Å)	1.5405981
Step scan increment (°2θ)	0.02
2θ range (°)	16–140
No. of reflections	575
No. of structural parameters	26
No. of profile parameters	18
No. of atoms	9
R_F	0.021
R_B	0.035
R_p	0.088
R_{wp}	0.113
R_{exp}	0.094

Note. The *R* factors are defined as

$$R_F = \frac{\Sigma|I(\text{"obs"})^{1/2} - I(\text{calc})^{1/2}|}{\Sigma I(\text{"obs"})^{1/2}},$$

$$R_B = \frac{\Sigma|I(\text{"obs"}) - I(\text{calc})|}{\Sigma I(\text{"obs"})},$$

$$R_p = \frac{\Sigma|y_i(\text{obs}) - (1/c)\, y_i(\text{calc})|}{\Sigma y_i(\text{obs})},$$

$$R_{wp} = \left[\frac{\Sigma\omega_i[y_i(\text{obs}) - (1/c)\, y_i(\text{calc})]^2}{\Sigma\omega_i[y_i(\text{obs})]^2}\right]^{1/2},$$

$$R_{exp} = \left[\frac{N - P}{\Sigma\omega_i[y_i(\text{obs})]^2}\right]^{1/2}.$$

TABLE 3
Positional and Thermal Parameters with Their Standard Deviations for $MoO_3 \cdot 1/2H_2O$

Atom	x	y	z	B_{iso} (Å^2)
Mo(1)	0.9870(2)	0.25	0.1946(2)	0.33(4)
Mo(2)	0.4190(2)	0.75	0.1512(2)	0.47(5)
O(1)	0.663(1)	0.75	0.302(1)	0.3(2)
O(2)	0.887(1)	0.25	0.368(2)	1.3(2)[a]
O(3)	0.973(1)	0.75	0.108(1)	−0.1(1)[b]
O(4)	0.159(1)	0.25	0.306(1)	0.0(2)
O(5)	0.470(1)	0.25	0.112(1)	−0.1(1)[b]
O(6)	0.752(1)	0.25	−0.003(2)	−0 1(2)
O(7)	0.384(1)	0.75	0.377(2)	1.3(2)[a]

Note. [a] and [b] indicate that some B_{iso} factors have been constrained to vary in the same manner.

O(6). This is often observed when the contrast between the scattering power of atoms is large and is partly due to the correlation of thermal parameters for light atoms with background level. These values have no physical meaning but they can be considered as statistically acceptable within 3 e.s.d.

RESULTS AND DISCUSSION

Figure 2 corresponds to a projection of the crystal structure of $MoO_3 \cdot 1/2H_2O$ parallel to [010], while Fig. 3 shows a projection parallel to [001]. They show that the structure is built up from layers parallel to (001) (Fig. 2). One layer may be described as an alternation of double linear rows, running along the [010] direction, of edge-sharing distorted octahedra [Mo(1)O_6] on one hand and [Mo(2)$O_5(H_2O)$] on the other hand (Fig. 3). Within a double chain, each octahedron MoO_6 has two common edges with its neighbors. So, in addition to the three bridge-formings by oxygen atoms (3 × O(3) for Mo(1) and 3 × O(5) for Mo(2)), Mo(1) is coordinated by two terminal oxygen atoms (O(2), O(4)), whereas Mo(2) is coordinated to only one terminal oxygen atom O(7) and one water molecule O(1). One oxygen atom O(6) common to two independent heavy atoms completes the coordination for Mo(1) and Mo(2). It means that the successive octahedral double chains are linked together by sharing corners to form a layer. Although the hydrogen atoms of the water molecule could not be located by means of the X-ray power diffraction method, it has been deduced from interatomic distances that O(1) must belong to the water molecule (Table 4).

As shown in Table 4, the two octahedra [Mo(1)O_6] and [Mo(2)$O_5(H_2O)$] exhibit significant distortions since their six Mo–O distances range from 1.68 to 2.40 Å and 1.71 to 2.37 Å. The corresponding mean values of 1.993 Å and 2.015 Å lie very close to the respective value for MoO_3 of 1.981 Å (26) and for α-$MoO_3 \cdot H_2O$ of 1.984 Å (4) or 1.975 Å (5). Regarding structural similarities between the three compounds, it can be suggested that the three structures are built up from very strongly distorted octahedra with a strong tendency toward fourfold coordination related to the ReO_3-type modification, as shown in Fig. 4. Whatever the octahedron nature ([MoO_6] for MoO_3 (26), [$MoO_5(H_2O)$] for α-$MoO_3 \cdot H_2O$ (4, 5), [MoO_6] and [$MoO_5(H_2O)$] for $MoO_3 \cdot 1/2H_2O$), the six interatomic Mo–O distances may be divided into three groups. The first group contains the two short distances close to 1.70 Å corresponding to the terminal oxygens (see Figs. 4a–4d) and the O(6^{II}) oxygen (see Fig. 4d) in $MoO_3 \cdot 1/2H_2O$. The second group concerns the two medium distances around 1.95 Å related to the bridge-forming oxygens (O(3), O(3^{I}) and O(5), O(5^{III}) of Mo(1)O_6 and

TABLE 4
Selected Interatomic Distances (Å) and Bond Angles (°) with Their Standard Deviations for $MoO_3 \cdot 1/2H_2O$

Mo(1)–O octahedron		Mo(2)–O octahedron	
Mo(1)–O(2)	1.72(1)	Mo(2)–O(1)	2.37(1)
Mo(1)–O(3)	1.948(1)	Mo(2)–O(5)	1.952(3)
Mo(1)–O(4)	1.68(1)	Mo(2)–O(6^{II})	1.76(1)
Mo(1)–O(6)	2.40(1)	Mo(2)–O(7)	1.71(1)
Mo(1)–O(3^{I})	1.948(1)	Mo(2)–O(5^{III})	1.952(3)
Mo(1)–O(3^{IV})	2.26(1)	Mo(2)–O(5^{II})	2.35(1)
O(2)–Mo(1)–O(3)	102.5(3)	O(1)–Mo(2)–O(5)	78.8(3)
O(2)–Mo(1)–O(3^{I})	102.5(3)	O(1)–Mo(2)–O(5^{III})	78.8(3)
O(2)–Mo(1)–O(3^{IV})	156.3(5)	O(1)–Mo(2)–O(5^{II})	77.2(3)
O(2)–Mo(1)–O(4)	108.4(5)	O(1)–Mo(2)–O(6^{II})	170.2(5)
O(2)–Mo(1)–O(6)	79.1(5)	O(1)–Mo(2)–O(7)	87.6(4)
O(3)–Mo(1)–O(3^{I})	143.9(5)	O(5)–Mo(2)–O(5^{III})	143.2(5)
O(3^{IV})–Mo(1)–O(3^{I})	73.3(3)	O(5)–Mo(2)–O(5^{II})	73.4(3)
O(3^{IV})–Mo(1)–O(3)	73.3(3)	O(5)–Mo(2)–O(6^{II})	98.6(3)
O(3^{IV})–Mo(1)–O(4)	95.3(4)	O(5)–Mo(2)–O(7)	103.9(3)
O(3^{IV})–Mo(1)–O(6)	77.2(4)	O(6^{II})–Mo(2)–O(7)	102.2(5)
O(3^{I})–Mo(1)–O(4)	98.1(3)	O(5^{III})–Mo(2)–O(5^{II})	73.4(3)
O(3^{I})–Mo(1)–O(6)	79.9(3)	O(5^{III})–Mo(2)–O(6^{II})	98.6(3)
O(3)–Mo(1)–O(4)	98.1(3)	O(5^{III})–Mo(2)–O(7)	103.9(3)
O(3)–Mo(1)–O(6)	79.9(3)	O(5^{II})–Mo(2)–O(6^{II})	93.0(5)
O(4)–Mo(1)–O(6)	172.5(5)	O(5^{II})–Mo(2)–O(7)	102.2(5)
Mo(1)–Mo(1) distances		Mo(2)–Mo(2) distances	
Mo(1)–Mo(1^{I})	3.70518(7)	Mo(2)–Mo(2^{I})	3.70518(7)
Mo(1)–Mo(1^{III})	3.70518(7)	Mo(2)–Mo(2^{III})	3.70518(7)
Mo(1)–Mo(1^{II})	3.380(2)	Mo(2)–Mo(2^{II})	3.455(3)
Mo(1)–Mo(1^{IV})	3.380(2)	Mo(2)–Mo(2^{IV})	3.455(3)
Posible hydrogen bonds			
O(1)–O(2)	2.81(1)	Mo(1)–O(2)–O(1)	114.2(4)
O(1)–O(7^{V})	3.04(1)	Mo(2)–O(1)–O(2)	137.1(2)
		Mo(2)–O(1)–O(7^{V})	92.6(3)
		O(2)–O(1)–O(7^{V})	72.9(3)

Note. Symmetry code: I, $x, -1 + y, z$; II, $1 - x, y + 0.5, -z$; III, $x, 1 + y, z$; IV, $1 - x, 0.5 - y, -z$; and V, $1 - x, 1 - y, 1 - z$.

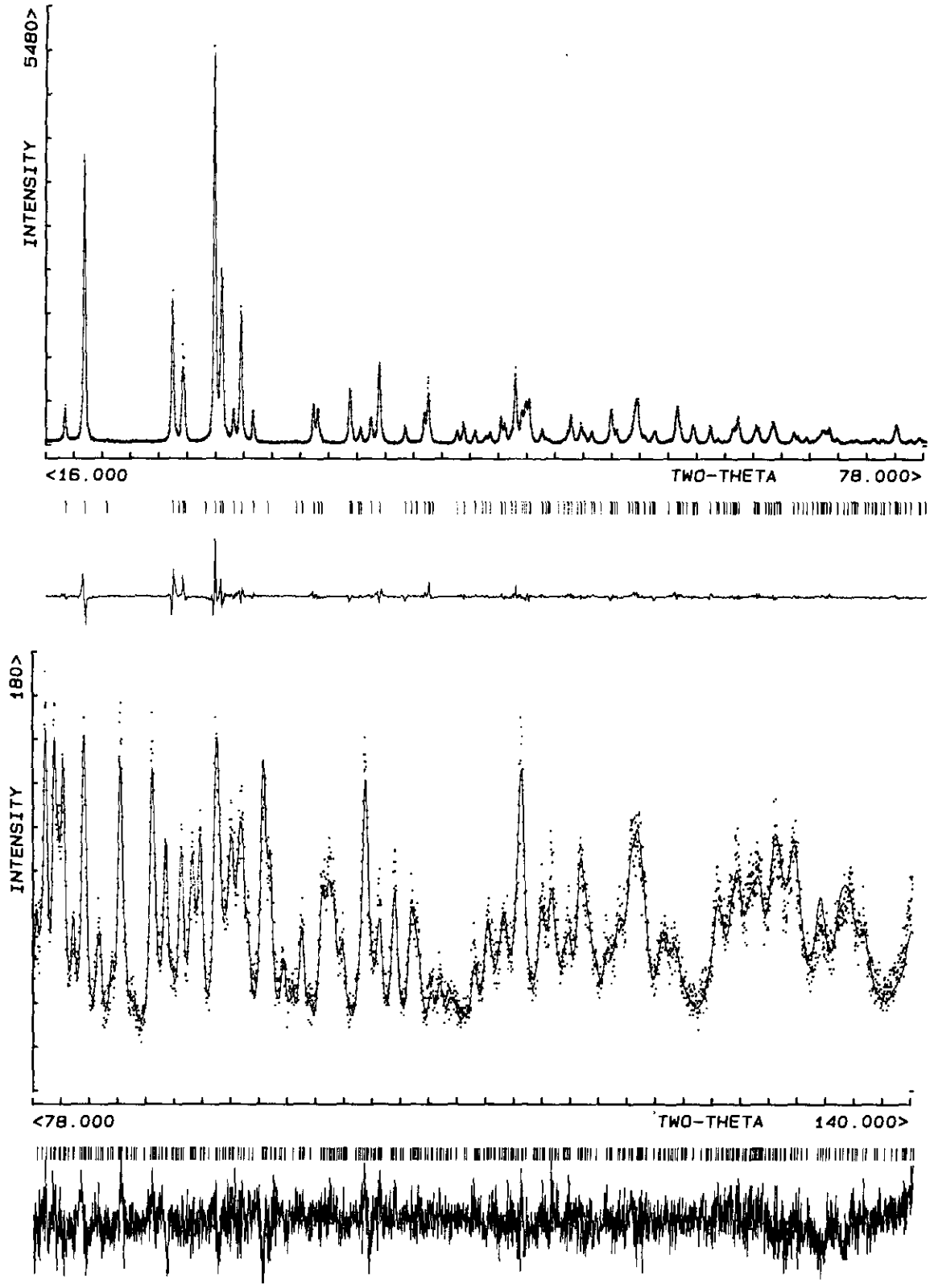

FIG. 1. The final Rietveld difference plot of $MoO_3 \cdot 1/2H_2O$. The upper trace shows the observed data as dots, while the calculated pattern is shown by the solid line. The lower trace is a plot of the difference: observed minus calculated. The vertical markers show positions calculated for Bragg reflections. Note that the intensity scale is different for the high angle range (bottom plot).

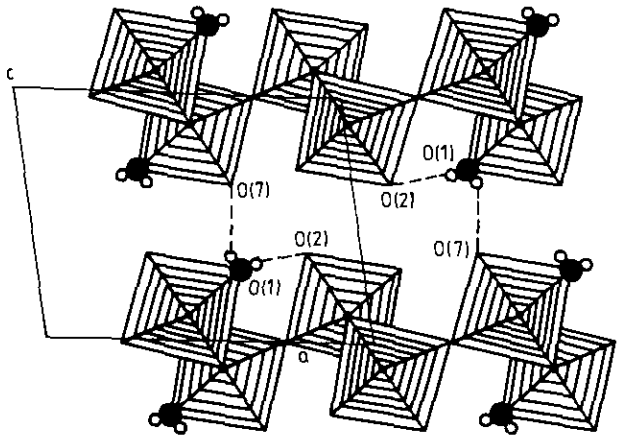

FIG. 2. Projection of the crystal structure of $MoO_3 \cdot 1/2H_2O$ parallel to [010] in terms of distorted octahedra sharing edges and corners. Probable hydrogen bonds are indicated by dotted lines.

$Mo(2)O_5(H_2O)$ in $MoO_3 \cdot 1/2H_2O$, respectively). Finally, two very long distances in the range from 2.26 to 2.40 Å, concerning the water oxygen (see Figs. 4b and 4d), the O(6) oxygen in $MoO_3 \cdot 1/2H_2O$ (see Fig. 4c) and in all cases the third bridging-oxygen atom ($O(3^{IV})$ and $O(5^{II})$ in $MoO_3 \cdot 1/2H_2O$), constitute the third group. It can be noted that the Mo(1)–O(6)–Mo(2) arrangement is characterized by a short and a long distance. This can be explained by the fact that O(6) is the oxygen which serves to link together two different rows in a layer.

From the O–O distances, as well as Mo–O–O and O–O–O angles around the water oxygen O(1), it is possible to look for hydrogen bonds within a layer and between two adjacent layers. These are represented by dotted lines in Fig. 2. It appears that the distance from O(1) to $O(7^V)$ (3.04 Å) is longer than the O(1)–O(2) distance (2.81 Å), which suggests that the forces holding each layer are greater than those holding the separate layers together. Moreover, it can be noted that the most possible hydrogen bonds correspond to the shortest Mo–O distances (Table 4).

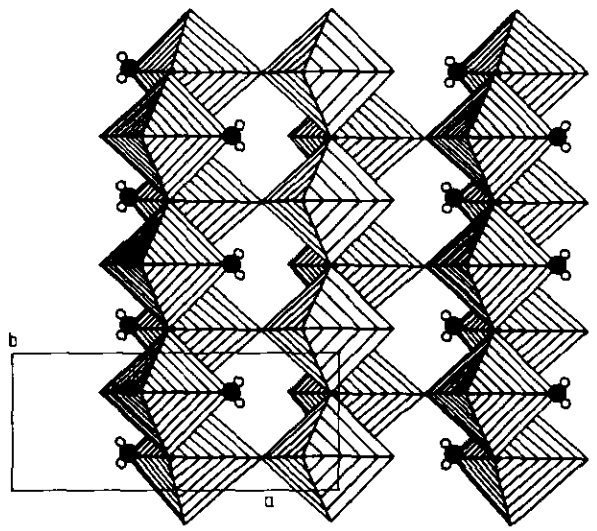

FIG. 3. Projection of the crystal structure of $MoO_3 \cdot 1/2H_2O$ parallel to [001] showing the layout of the octahedra in a layer.

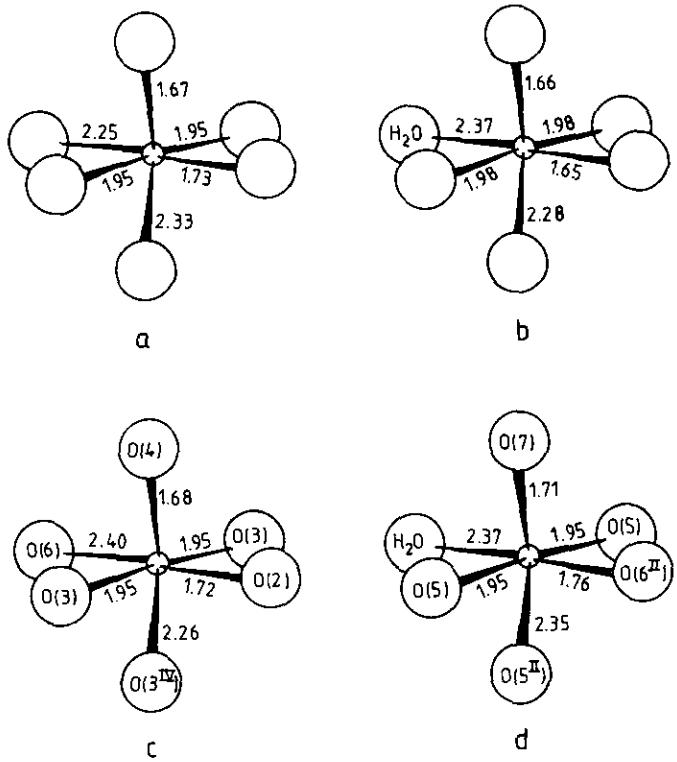

FIG. 4. Coordination sphere of oxygen atoms around the Mo atoms in (a) MoO_3 (26) [MoO_6]; (b) α-$MoO_3 \cdot H_2O$ (5) [$MoO_5(H_2O)$]; (c) $MoO_3 \cdot 1/2H_2O$ [MoO_6]; and (d) $MoO_3 \cdot 1/2H_2O$ [$MoO_5(H_2O)$].

Several hydrates and oxides are known for $WO_3 \cdot xH_2O$ and $MoO_3 \cdot xH_2O$ with $x = 2$, 1, 1/2, and 0. The structures of tungsten oxide hydrates (27–31) are described only from corner-sharing octahedra, while for molybdenum oxide hydrates (2–6), some of them are built from corner- and edge-sharing octahedra, as we have exemplified for $MoO_3 \cdot 1/2H_2O$. This difference can be explained by the stronger (p_π–d_π) interaction in the case of molybdenum, which leads to more distorted octahedra.

REFERENCES

1. F. Hulliger, *in* "Structural Chemistry of Layer-Type Phases" (F. Lévy, Ed.), Vol. 5. Reidel, Dordrecht, 1976.
2. B. Krebs, *Chem. Commun.*, 50 (1970).
3. B. Krebs, *Acta Crystallogr. Sect. B* **28**, 2222 (1972).
4. V. Böschen and B. Krebs, *Acta Crystallogr. Sect. B* **30**, 1795 (1974).

5. H. R. Oswald, J. R. Günter, and E. Dubler, *J. Solid State Chem.* **13,** 330 (1975).
6. J. R. Günter, *J. Solid State Chem.* **5,** 354 (1972).
7. F. Harb, B. Gerand, G. Nowogrocki, and M. Figlarz, *C. R. Acad. Sci. Paris* **303**(II), 349 (1986); *Solid State Ionics* **32–33,** 84 (1989).
8. R. L. Fellows, M. H. Lloyd, J. F. Knight, and H. L. Yakel, *Inorg. Chem.* **22,** 2468 (1983).
9. J. P. Attfield, A. W. Sleight, and A. K. Cheetham, *Nature (London)* **322,** 620 (1986).
10. P. Lightfoot, A. K. Cheetham, and A. W. Sleight, *Inorg. Chem.* **26,** 3544 (1987).
11. A. Clearfield, L. B. McCusker, and P. R. Rudolf, *Inorg. Chem.* **23,** 4679 (1984).
12. D. Louër and M. Louër, *J. Solid State Chem.* **68,** 292 (1987).
13. P. Bénard, M. Louër and D. Louër, *J. Solid State Chem.* **94,** 27 (1991).
14. D. Louër and J. I. Langford, *J. Appl. Crystallogr.* **21,** 430 (1988).
15. D. Louër and M. Louër, *J. Appl. Crystallogr.* **5,** 271 (1972).
16. A. Boultif and D. Louër, *J. Appl. Crystallogr.* **24,** 987 (1991).
17. P. M. De Wolff, *J. Appl. Crystallogr.* **1,** 108 (1968).
18. G. S. Smith and R. L. Snyder, *J. Appl. Crystallogr.* **12,** 60 (1979).
19. A. D. Mighell, C. R. Hubbard, and J. K. Stalick, "NBS*AIDS80: A FORTRAN Program for Crystallographic Data Evaluation." Nat. Bur. Stand. (U.S.A.) Tech. Note 1141, 1981. [NBS*AIDS83 is an expanded version of NBS*AIDS80]
20. D. Louër, *Mater. Sci. Forum* **79–82,** 17 (1991).
21. A. Le Bail, H. Duroy, and J. L. Fourquet, *Mater. Res. Bull.* **23,** 447 (1988).
22. J. Rodriguez-Carvajal, in "Collected Abstracts of Powder Diffraction Meeting, Toulouse, France, July 1990," p. 127.
23. D. B. Wiles, A. Sakthivel, and R. A. Young, *in* "User's Guide to Program DBW3.2S (version 8804)." Georgia Institute of Technology, Atlanta, 1988.
24. D. B. Wiles and R. A. Young, *J. Appl. Crystallogr.* **14,** 149 (1981).
25. "Structure Determination Package" (*MolEN*). Enraf–Nonius, Delft, The Netherlands, 1990.
26. L. Kihlborg, *Ark. Kemi* **21,** 357 (1963).
27. M. L. Freedman, *J. Am. Chem. Soc.* **81,** 3834 (1959).
28. J. T. Szymansky, *Can. Miner.* **22,** 681 (1984).
29. B. Gerand, G. Nowogrocki, and M. Figlarz, *J. Solid State Chem.* **38,** 312 (1981).
30. G. Andersson, *Acta Chem. Scand.* **7,** 154 (1953).
31. S. J. Tanisaki, *Phys. Soc. Jpn.* **15,** 573 (1960).